

Chemical Science

Accepted Manuscript

This article can be cited before page numbers have been issued, to do this please use: H. Zhang, M. Zhang, H. Zhuo, H. Yang, B. Han, Y. Zheng, H. Wang, H. Lin, S. Tao, C. Zheng and X. Zhang, *Chem. Sci.*, 2024, DOI: 10.1039/D4SC03667K.



This is an Accepted Manuscript, which has been through the Royal Society of Chemistry peer review process and has been accepted for publication.

Accepted Manuscripts are published online shortly after acceptance, before technical editing, formatting and proof reading. Using this free service, authors can make their results available to the community, in citable form, before we publish the edited article. We will replace this Accepted Manuscript with the edited and formatted Advance Article as soon as it is available.

You can find more information about Accepted Manuscripts in the [Information for Authors](#).

Please note that technical editing may introduce minor changes to the text and/or graphics, which may alter content. The journal's standard [Terms & Conditions](#) and the [Ethical guidelines](#) still apply. In no event shall the Royal Society of Chemistry be held responsible for any errors or omissions in this Accepted Manuscript or any consequences arising from the use of any information it contains.

ARTICLE

Unraveling Non-Radiative Decay Channels of Exciplexes to Construct Efficient Red Emitters for Organic Light-Emitting Diodes

Heng-Yuan Zhang,^a Ming Zhang,^a Hao Zhuo,^a Hao-Yu Yang,^a Bo Han,^{*b} Yong-Hao Zheng,^a Hui Wang,^c Hui Lin,^a Si-Lu Tao,^a Cai-Jun Zheng,^{*a} and Xiao-Hong Zhang^{*c}

Received 00th January 20xx,
Accepted 00th January 20xx

DOI: 10.1039/x0xx00000x

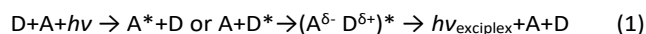
Exciplex emitters naturally have thermally activated delayed fluorescence characteristics due to their spatially separated molecular orbitals. However, the intermolecular charge transfer potentially induces diverse non-radiative decay channels, severely hindering the construction of efficient red exciplexes. Thus, a thorough comprehension of this energy loss is of paramount importance. Herein, different factors, including molecular rigidity, donor-acceptor interactions and donor-donor/acceptor-acceptor interactions, that impact the non-radiative decay were systematically investigated using contrasting exciplex emitters. The exciplex with rigid component and intermolecular hydrogen bonds showed photoluminescence quantum yield of 84.1% and singlet non-radiative decay rate of $1.98 \times 10^6 \text{ s}^{-1}$ under optimized mixing ratio, respectively achieving a 3.3-fold increase and a 70% decrease than the comparison group. In the electroluminescence device, a maximum external quantum efficiency of 23.8% was achieved with an emission peak of 608 nm, which represents the state-of-the-art organic light-emitting diodes using exciplex emitters. Accordingly, a new strategy is finally proposed, exploiting system rigidification to construct efficient red exciplex emitters that suppress the non-radiative decay.

Introduction

The excited complex, known as the exciplex, has been considered detrimental to the efficiency of organic light-emitting diodes (OLEDs) since Karasz et al. first observed the unexpected and extra red-shifted emission in 1994.¹ It was not until 2012 when Adachi and coworkers² reported the thermally activated delayed fluorescence (TADF) characteristic of some exciplexes that researchers began to probe their applications in OLEDs.^{3–9} Formed by mixing electron donors and electron acceptors (D:A) to generate intermolecular charge-transfer (CT) states, the exciplexes possess small singlet-triplet energy gaps (ΔE_{ST}) because of the spatially separated highest occupied molecular orbitals (HOMO) and lowest unoccupied molecular orbitals (LUMO), which promotes the reverse intersystem crossing (RISC), converting dark triplet excitons to singlet excitons. Benefiting from the theoretical 100% exciton utilization, TADF exciplex emitters are promising to achieve efficient electroluminescence (EL).

Over the past decade, with considerable efforts in molecular design and combination optimization of D:A pairs, blue and green OLEDs that utilize exciplex emission have realized

remarkable maximum external quantum efficiencies (EQE_{max}) of 20.43%¹⁰ and 26.4%¹¹, respectively. However, the efficiency of red exciplex emitters is far from satisfactory. The highest EL efficiency up to date was contributed by Cheng et al., realizing an EQE_{max} of 14.6% with an emission peak at 592 nm.¹² When the emission peak is limited to redder than 600 nm, the highest EQE_{max} (8.68%) was achieved by using a manganese-based donor and a beryllium-based acceptor.¹³ Besides, researchers combined stronger donors and acceptors for deep-red and near-infrared emission, but the EQE_{max} s were less than 5%.^{14–16} As summarized above, a clear trend can be observed, that is a sharp decrease in efficiency with the redshifts of emission, which can be mainly ascribed to the exponentially increasing non-radiative energy loss as the energy gap gets smaller.¹⁷ Therefore, the inhibition of such energy loss is imperative in realizing efficient red exciplexes, as evidenced by the extensive research on single-molecule red TADF emitters.^{18–20} Theoretically, the emitting process of an exciplex can be described as:⁵



where a donor (or an acceptor) is excited first and then collides with a ground-state acceptor (or donor) to generate CT states prior to the final emission. All the processes should be taken into account to study the emission mechanisms of exciplexes.^{7,21} As a result, the non-radiative decay should be considered during the excitation of D or A, the CT between D and A molecules and the final radiation. The properties of the constituting molecules and the D-A intermolecular interactions are therefore influential to the exciplex emission.⁸ Besides, as the mixing ratios of D and A in an exciplex system are generally

^a School of Optoelectronic Science and Engineering, University of Electronic Science and Technology of China, Chengdu 611731, P. R. China. Email: zhengcaijun@uestc.edu.cn

^b Chengdu University of Traditional Chinese Medicine, State Key Laboratory Southwestern Chinese Medicine Resources, Chengdu 611137, P. R. China. Email: hanbo@cdutcm.edu.cn

^c Institute of Functional Nano & Soft Materials (FUNSOM), Soochow University, Suzhou 215123, P. R. China. Email: xiaohong_zhang@suda.edu.cn

Supplementary Information available: [details of any supplementary information available should be included here]. See DOI: 10.1039/x0xx00000x



similar (many are even mixed in equal proportions), the non-radiative energy loss caused by concentration quenching should also be noticed, especially for red exciplexes where the efficiency is substantially constrained by such energy loss. Consequently, the D:A-type exciplex emitters potentially possess more non-radiative decay channels (Figure 1A) compared with the single-molecule TADF emitters. And it is of vital significance to unravel specific paths and propose effective strategies to construct efficient red exciplex emitters.

In this work, we systematically investigate non-radiative decay channels of red exciplex emitters using contrasting D:A pairs and propose an effective strategy accordingly. As shown in Figure 1B, two donors and three acceptors were developed using phenoxazine/phenothiazine (PXZ/PTZ) and N-heterocycles to achieve red emission and all six exciplexes show emission peaks around 600 nm. The three acceptors are distinguished by their attachments that the spiro-locked SAF-2NP is much more rigid than triphenylamine (TPA)-based TPA-2NP and TPA-QP. Additionally, the regulation of intermolecular interactions between D and A molecules was achieved by strategic molecular design. Intermolecular hydrogen bonds (HBs) between PXZ and 2NP were found in mPTBC:SAF-2NP and mPTBC:TPA-2NP because of the exposing electronegative sites while mPTBC:TPA-QP, mPTZC:SAF-2NP, mPTZC:TPA-2NP and mPTZC:TPA-QP lack corresponding interactions. It was found that both suppressing the structural relaxation of exciplex components and strengthening D-A interactions are beneficial for restricting non-radiative decay. Owing to the synergy of stable structures and intermolecular HBs, mPTBC:SAF-2NP showed the lowest k_{nr} (singlet non-radiative decay rates, $1.98 \times 10^6 \text{ s}^{-1}$) and the largest photoluminescence quantum yield (PLQY, 84.1%) among the six exciplexes. Further, the D-D/A-A interactions were studied. Suffering from exciton quenching caused by π - π stacking of SAF-2NP, k_{nr} of mPTBC:SAF-2NP gradually rose as the acceptor concentration increased. The concentration quenching was much more severe in TPA-containing exciplex emitters. Moderate efficiency declines of mPTBC:SAF-2NP-based devices were observed where EQE_{max}s maintain above 20% with D:A ratio from 9:1 to 6:4. Under the optimized ratio, an outstanding EQE_{max} of 23.8% with an emission peak at 608 nm was obtained, which not only surpasses all previously reported red exciplex OLEDs but also ranks among state-of-the-art exciplex-emissive devices. Based on the above results, we elucidate that the molecular rigidity, D-D/A-A interactions and D-A interactions are three factors that impact the non-radiative decay. Accordingly, we propose a new strategy leveraging a rigid system featuring stiff structures, intermolecular HBs and optimized D:A ratio to construct red exciplex emitters that effectively suppresses the non-radiative decay. The present work provides perspectives to understand the non-radiative decay paths and is helpful to elucidating the emission mechanisms of exciplex emitters.

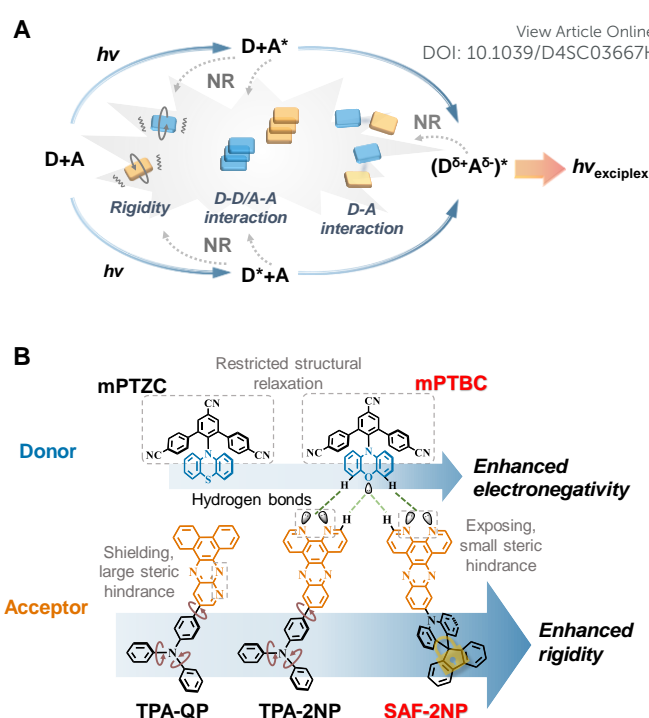


Figure 1. (A) Illustration of the emitting process of exciplex emitters and three factors that can lead to non-radiative decay of exciplex emitters. D stands for donors; A represents acceptors and NR is non-radiative decay. (B) Design concept and corresponding molecular structures of donors and acceptors.

Results and discussion

Exciplex construction and molecular characterization

The donor-acceptor structure was applied to construct exciplex constituents, which induces TADF characteristic and thus improves exciton utilization of exciplex systems. mPTBC was constructed by incorporating PXZ onto a sterically crowded group. The V-shaped tri-benzonitrile on the one hand, obstructs the rotation of PXZ and minimizes the structure deformation; on the other hand, prevents planar PXZ from π - π stacking. The acceptor SAF-2NP was a bulky and planar N-heterocycles modified with an sp³ hybridized carbon mediated orthogonal spiro-acridine unit, which locks the rotational peripheries. To regulate the constituent rigidity and D-A intermolecular interactions, as for the donor, PTZ is substituted for PXZ to produce mPTZC, resulting in a decrease in electronegativity²² and a moderate alteration in the HOMO energy level. This greatly lowers the possibility of HB formation since weak HB is dominated by electrostatic interaction.²³ As for the acceptors, by replacing SAF with the TPA unit, the structural stability is greatly impaired because of the rotatable attachments and reduced steric hindrance between TPA and 2NP/QP.²⁴ In addition, the position of nitrogen atoms of QP is elaborately modified from exposing to shielding sites of the molecule (Figure 1B), generating large steric hindrance for HB formation compared with 2NP.

2'-(10H-phenoxazin-10-yl)-[1,1':3',1''-terphenyl]-4,4'',5'-tricarbonitrile (mPTBC),²⁵ 10-(dipyrido[3,2-a:2',3'-c]phenazin-11-yl)-10H-spiro[acridine-9,9'-fluorene] (SAF-2NP),²⁶ 4-(dipyrido[3,2-



a:2',3'-c]phenazin-11-yl)-N,N-diphenylaniline (TPA-2NP)²⁷ and 4-(dibenzo[f,h]pyrido[2,3-b]quinoxalin-12-yl)-N,N-diphenylaniline (TPA-QP)²⁸ were synthesized according to previous reports. 2'-(10H-phenoxazin-10-yl)-[1,1':3',1''-terphenyl]-4,4'',5'-tricarbonitrile (mPTZC) was readily synthesized using the same procedure as mPTBC, including Suzuki coupling, diazotization reaction and C-N cross-coupling of tri-benzonitrile and PTZ. Column chromatography, recrystallization and sublimation were used to obtain appreciable purity. Its chemical structure was fully characterized through ¹H and ¹³C nuclear magnetic resonance (NMR) spectroscopy and mass spectrometry. The basic physical properties of donors and acceptors were characterized first (summarized in Table S1). Thermogravimetric analysis (TGA) and differential scanning calorimetry (DSC; Figure S1) tests were conducted to evaluate the thermal stability of mPTZC. The decomposition temperature (corresponding to 5% weight loss) of mPTZC is calculated to be 381 °C and no glass transition was observed. As shown in Figure S2, mPTZC, TPA-2NP and TPA-QP show clear CT absorption and emission peaks around 430 nm and 540 nm, respectively. According to the fluorescence and phosphorescence spectra, TPA-2NP and TPA-QP possess relatively large ΔE_{STS} due to the large conjugation, similar to other TPA-based TADF emitters.^{19,29,30} On the contrary, twisted structures of mPTBC, mPTZC and SAF-2NP induce tiny ΔE_{STS} , which may further affect the fluorescence lifetime and RISC rates of the corresponding exciplexes. Estimated according to the reduction and oxidation curves (Figure S3) obtained by cyclic voltammetry method, SAF-2NP, TPA-2NP and TPA-QP have similar LUMO energy levels of -3.32 eV, -3.27 eV and -3.31 eV, respectively. mPTBC and mPTZC show similar HOMO energy levels, making the corresponding exciplex emitters comparable. The fluorescence spectra of the six exciplex emitters and their electron-donating and electron-accepting components are displayed in Figure S4 and S5. Emission peaks at around 600 nm were observed for all six exciplexes, exhibiting clear red shifts compared with those of their constituents, confirming the exciplex formation.³¹ The emission energy is in accordance with the differences between HOMO energy levels of donors and LUMO energy levels of acceptors (listed in Table S1).

Molecular rigidity and intermolecular interactions

In order to theoretically distinguish the rigidity of these compounds, density functional theory (DFT) and time dependent-DFT (TD-DFT) were conducted using Gaussian.³² As shown in Figure 2A, optimized geometries of the ground state (S_0), the lowest singlet excited state (S_1) and the lowest triplet state (T_1) of as well as corresponding root-mean-square displacements (RMSD) of all five components were calculated using VMD³³ in the first place. There is little geometry change between the ground state and excited states for mPTBC and mPTZC, indicating the V-shaped tri-benzonitrile effectively stabilizes the molecules. As for the acceptors, RMSD show a prominently decreasing trend from TPA-QP to SAF-2NP, indicating suppressed structural relaxation. These larger values of TPA-modified acceptors mainly arise from dihedral angles change between TPA and 2NP/QP as well as the rotation of peripheral phenyl. To further study the structural deformation, Huang-Rhys factors at different normal mode frequencies of the

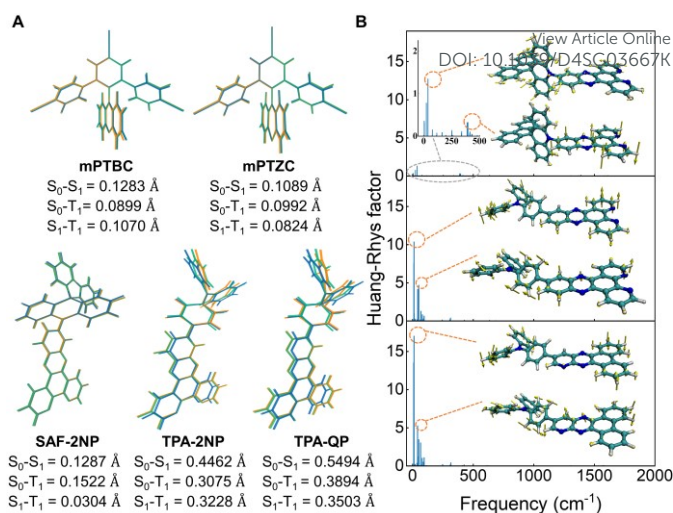


Figure 2. (A) S_0 , S_1 and T_1 (in blue, orange and green, respectively) geometry variations of the five monomers and corresponding RMSD values. (B) Calculated S_0-S_1 Huang-Rhys factors of SAF-2NP (upper), TPA-2NP (middle) and TPA-QP (lower) at different frequencies (insert: representative vibrational modes).

three acceptors were calculated according to the reorganization energy using the DUSHIN program³⁴ and the results are demonstrated in Figure 2B and Figure S6. The Huang-Rhys factor of SAF-2NP is significantly smaller than those of TPA-2NP and TPA-QP. Inserted in Figure 2B, the most and second most representative normal modes of SAF-2NP correspond to wagging vibrations of the acridine unit (38 cm⁻¹) and C-H as well as C-C twisting vibrations of the 2NP plane (396 cm⁻¹). While TPA-2NP and TPA-QP possess similar twisting vibration modes resulting in rotations between the peripheral phenyl and the acceptor plane (12 cm⁻¹) as well as rotations between the acceptor plane and adjacent phenyl (51 cm⁻¹). Besides, the primary vibrations that contribute to the reorganization energy of SAF-2NP and TPA-derivates respectively belong to the high-frequency region which corresponds to bond length change and the low-frequency region that relates to dihedral angle change (Figure S6).²⁴ The relatively smaller reorganization energy of SAF-2NP is derived from the effective suppression of low-frequency vibrations. The above data well support our molecular design that SAF-2NP is rigidified by restricting D-A rotations using acridine with large steric hindrance and locking the flexible benzene with fluorene. Therefore, it is rational to explore the influence of structural stiffness on the non-radiative decay of exciplexes using SAF-2NP, TPA-2NP and TPA-QP as acceptors.

Moreover, the D-A intermolecular interactions were investigated experimentally and theoretically. Based on our molecular design concept, mPTZC and TPA-QP cannot form the desired intermolecular HBs in exciplex systems. The assumption was initially verified using fitted atomic charges of the five molecules. As shown in Figure S7, although the maximum hydrogen charges of mPTBC and mPTZC are similar, respectively locating near oxygen and sulfur, the oxygen charge are two times more negative than the sulfur charge, providing feasibility for stronger interactions. For SAF-2NP and TPA-2NP, nitrogen atoms in phenanthroline have the most negative charges and the exposing sites benefit the formation of intermolecular HBs



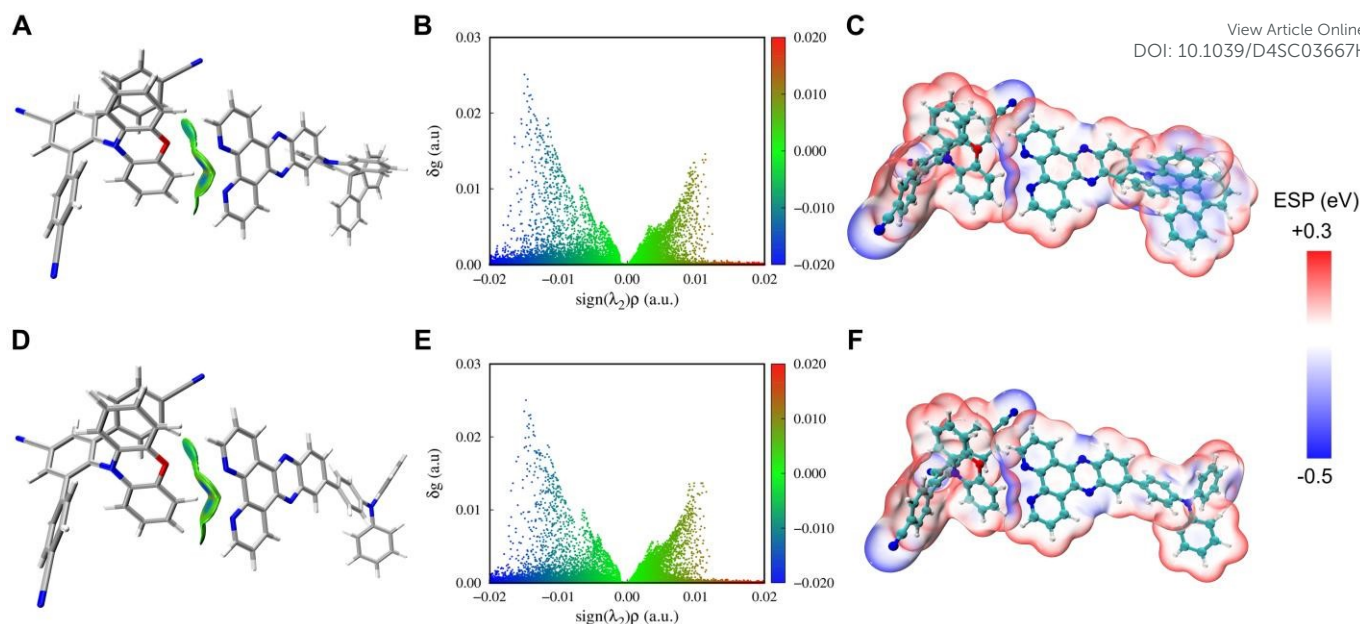


Figure 3. Isosurface maps of intermolecular interaction based on optimized geometry (isovalue = 0.003 a.u., color range ± 0.02 a.u.), corresponding scatter plots and ESP maps of mPTBC:SAF-2NP (A-C) and mPTBC:TPA-2NP (D-F)

between PXZ and 2NP in mPTBC:SAF-2NP and mPTBC:TPA-2NP. In contrast, the electronegative nitrogen atoms of TPA-QP are shielded by TPA and phenanthrene groups, generating large steric hindrance. The restrained electrostatic potential (RESP) was also used (Figure S8), which showed good consistency with the MK method. Fourier Transform infrared (FT-IR) spectra were recorded to make experimental validation (Figure S9). New absorption peaks at 2967 and 2962 cm^{-1} are respectively observed for mPTBC:SAF-2NP and mPTBC:TPA-2NP, which are shifted from the C-H stretching modes (around 3059 cm^{-1}), demonstrating the existence of intermolecular HBs.^{35,36} Meanwhile, the spectra of the other four blends are the superposition of the components. To better illustrate the intermolecular interactions of mPTBC:SAF-2NP and mPTBC:TPA-2NP, the independent gradient model based on Hirshfeld partition (IGMH)³⁷ analysis was carried out using Multiwfn³⁸ based on the optimized geometries. As shown in Figure 3A, B, D and E, the blue region in the isosurface and scatter plots denotes attractive interaction and the green region represents dispersion-dominant interaction. Prominent C-H...N intermolecular HBs are observed with the participation of the active hydrogen next to oxygen and two strong-electronegativity nitrogen atoms (Figure S10). The central area of C-H...O isosurface appear lighter blue, indicating the interactions are weaker than C-H...N, but it is also helpful to stabilize the exciplex system. The interaction energy was respectively calculated to be -10.09 and -10.19 kcal/mol for mPTBC:SAF-2NP and mPTBC:TPA-2NP considering the basis set superposition error (BSSE), which is in a range of weak intermolecular HBs.²³ The interaction region in the electrostatic potential (ESP) map³⁹ (Figure 3C and F) exhibits red-blue crossings, in line with the previous report that weak HBs are dominated by electrostatic interaction. Intermolecular HBs may

benefit the interactions between D and A molecules, facilitating the exciplex formation. Moreover, the exciplex systems can be stabilized, weakening the non-radiative decay.

Based on the above analysis, molecular rigidity and intermolecular interactions are modified by elaborate molecular design. And the pairwise combination of D:A can be fitted into the following four scenarios. mPTBC:TPA-QP, mPTZC:TPA-2NP and mPTZC:TPA-QP contain the relatively flexible TPA segments. Besides, the weak electronegativity of sulfur in mPTZC and shielding nitrogen in TPA-QP impede the formation of desired HBs. Therefore, these three exciplexes stand for circumstances that lack both constituent rigidity and effective intermolecular HBs. Likewise, mPTZC:SAF-2NP is expected to have no intermolecular HBs between PTZ and 2NP while good rigidity is anticipated. mPTBC:TPA-2NP possesses favorable HBs but serious structural relaxation. Impressively, both were achieved for the proof-of-concept mPTBC:SAF-2NP, which is expected to effectively inhibit the non-radiative decay and achieve efficient red emission.

Photophysical properties

The transient photophysical properties of the six exciplexes were then characterized to study the exciton dynamics. Given the twisted structure of donors and planar geometry of acceptors, the D:A mixing ratio for all six exciplexes was set to be 9:1 in the first place to avoid concentration quenching. As shown in Figure 4A, S9 and Table 1, nanosecond-scale prompt decay lifetime (τ_p) and microsecond-scale delayed fluorescence lifetime (τ_d) were obtained for all six exciplexes, validating their TADF characteristic. Note that the multiple RISC channels in all six exciplex systems lead to complexity of the emission processes.⁴⁰ Herein we focus on the overall decay characteristic rather than classification of specific emitting species. TPA-containing exciplexes have larger τ_d s, which can be ascribed to



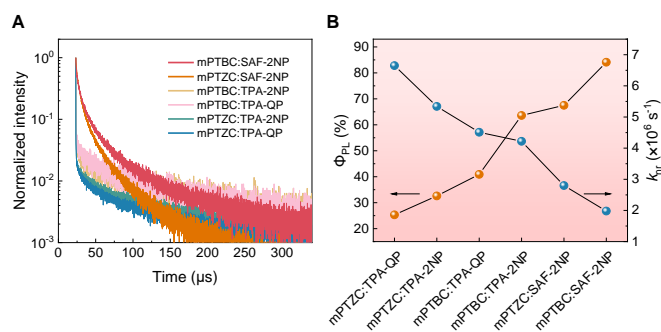


Figure 4. (A) PL decay curves of mPTBC:SAF-2NP, mPTZC:SAF-2NP, mPTBC:TPA-2NP, mPTBC:TPA-QP, mPTZC:TPA-2NP and mPTZC:TPA-QP. (B) Variation trends of Φ_{PL} and k_{nr} from mPTZC:TPA-QP to mPTBC:SAF-2NP (D:A = 9:1).

their larger ΔE_{STs} (Figure S12). And the longer τ_{dS} of TPA-2NP and TPA-QP compared with that of SAF-2NP (Figure S13) are also responsible since this leads to longer triplet lifetimes in the exciplex systems. The significantly smaller τ_d of SAF-2NP compared with TPA-based acceptors contributes to shorter τ_{dS} of mPTBC:SAF-2NP (22.3 μs) and mPTZC:SAF-2NP (17.5 μs). An increasing trend of Φ_{PL} and a decreasing trend of k_{nr} from mPTZC:TPA-QP to mPTBC:SAF-2NP, as observed in Figure 4B. mPTBC:TPA-QP, mPTZC:TPA-2NP and mPTZC:TPA-QP have large k_{nr} s and non-radiative decay is gradually reduced after introducing HBs (mPTBC:TPA-2NP) and the stiff acceptor (mPTZC:SAF-2NP). mPTBC:SAF-2NP possesses the smallest k_{nr} . Specifically, in terms of structure rigidification, k_{nr} s are respectively decreased by 57.9% and 47.6% from mPTZC:TPA-QP ($6.65 \times 10^6 \text{ s}^{-1}$) and mPTZC:TPA-2NP ($5.34 \times 10^6 \text{ s}^{-1}$) to mPTZC:SAF-2NP ($2.80 \times 10^6 \text{ s}^{-1}$). Similarly, a drop rate of 53.1% are obtained from mPTBC:TPA-2NP to mPTBC:SAF-2NP. These improvements can be attributed to the bulky acridine and periphery-locking fluorene, which effectively curbs the structural deformation. TPA-QP-based exciplexes have larger k_{nr} s than those containing TPA-2NP, which can be ascribed to

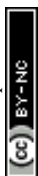
more severe structural relaxation of TPA-QP (Figure 2). Comparatively, the introduction of HBs has less effect on k_{nr} . It is respectively decreased by 29.3% and 6.4% from mPTZC:SAF-2NP ($2.80 \times 10^6 \text{ s}^{-1}$) to mPTBC:SAF-2NP ($1.98 \times 10^6 \text{ s}^{-1}$) and from mPTBC:TPA-QP ($4.51 \times 10^6 \text{ s}^{-1}$) to mPTBC:TPA-2NP ($4.22 \times 10^6 \text{ s}^{-1}$). This experimentally validates our assumption that intermolecular HBs can rigidify the exciplex systems and weaken non-radiative decay. The enhancement of k_f of mPTBC:TPA-2NP compared with that of mPTZC:SAF-2NP may originate from the large conjugation of TPA-2NP. Remarkably, mPTBC:SAF-2NP has the largest Φ_{PL} of 84.1% and the smallest k_{nr} , showing a 3.3-fold increase and a 70% decrease compared with those of mPTZC:TPA-QP. According to these results, improving the component stiffness has a dramatic impact on the non-radiative decay of the exciplex systems while intermolecular HBs have relatively moderate influence and barely work for systems that lack sufficient structural stability. The impressive performance of mPTBC:SAF-2NP highlights the significance of synergy of rigid structures and strong intermolecular interactions that effectively suppress non-radiative transition.

According to the above studies, the molecular rigidity of red exciplex emitters is the basis for suppressing non-radiative decay. Planar structures are therefore hard to avoid and the consequent concentration quenching would be no longer negligible. Steady-state PL spectra, Φ_{PL} and transient PL curves of mPTBC:SAF-2NP with D:A ratios from 9:1 to 6:4 were measured. Both τ_p and τ_d remain nearly identical (Figure S14 and Table S2) with the increasing concentration of SAF-2NP. While Φ_{PL} shows a decreasing trend, making k_{nr} gradually increases from $1.98 \times 10^6 \text{ s}^{-1}$ to $2.72 \times 10^6 \text{ s}^{-1}$. The photophysical properties of other five exciplexes with different D:A ratios were also studied (Figure S15 and Table S3). The k_{nr} s of TPA-containing exciplexes are much more sensitive to the concentration, demonstrating 1.2~1.7-fold increases from D:A = 9:1 to 8:2. While the concentration of SAF-2NP has smaller alterations.

Table 1. Summary of photophysical properties of the six exciplexes.

Emitter	$\lambda_{PL}^{a,b)}$ [nm]	$\Phi_{PL}^{b,c)}$ [%]	$\tau_p^{b)}$ [ns]	$\tau_d^{b)}$ [μs]	k_f [10^6 s^{-1}]	$k_{ISC}^{d)}$ [10^7 s^{-1}]	$k_{RISC}^{f)}$ [10^5 s^{-1}]	$k_{nr}^{g)}$ [10^6 s^{-1}]
mPTBC:SAF-2NP	610	84.1	20.7	22.3	10.50	3.57	1.74	1.98
mPTZC:SAF-2NP	608	67.5	23.2	17.5	5.82	3.43	2.86	2.80
mPTBC:TPA-2NP	596	63.6	18.7	65.2	7.04	4.18	0.71	4.22
mPTBC:TPA-QP	610	40.9	21.3	59.6	3.12	3.92	1.03	4.51
mPTZC:TPA-2NP	600	32.6	15.5	77.7	2.58	5.65	1.05	5.34
mPTZC:TPA-QP	608	25.3	13.9	62.6	2.25	6.29	1.29	6.65

^{a)} Emission peaks of fluorescence spectra. ^{b)} Measured with exciplex solid films (D:A = 9:1). ^{c)} Measured in a nitrogen atmosphere. ^{d)} Intersystem crossing rate constant. ^{f)} RISC rate constant. ^{g)} Singlet non-radiative decay rate constant.



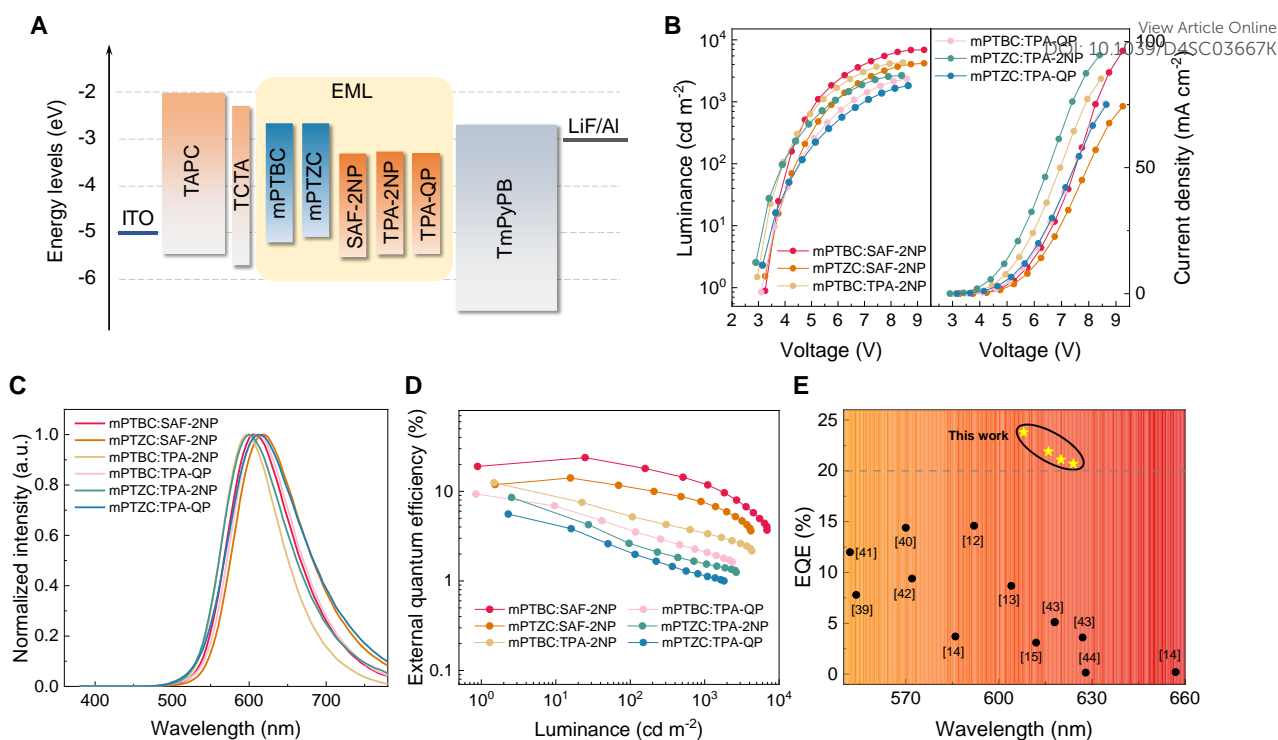


Figure 5. (A) Device configuration of the exciplex-based OLEDs. Luminance-voltage-current density curves (B), EL spectra (C) and EQE-luminance plot (D) of mPTBC:SAF-2NP, mPTBC:TPA-2NP, mPTZC:SAF-2NP, mPTZC:TPA-2NP and mPTZC:TPA-QP. (E) EQE vs. wavelength plot of representative yellow to deep-red OLEDs based on exciplex emitters.

To understand these results, the crystal structures and corresponding packing modes of mPTBC (CCDC 2343106), SAF-2NP (CCDC 2343111) and TPA-QP (CCDC 2370557) are demonstrated. As shown in Figure S16, for mPTBC, the stacking of PXZ is effectively avoided by the two carbonitrile arms. No π - π interactions but only C-H...N and C-H... π interactions were observed. For the acceptors (Figure S17), SAF-2NP has head-to-tail stacking with larger intermolecular distances of ~ 3.33 and

~ 3.45 Å while TPA-QP shows head-to-head off-center parallel stacking with intermolecular distances of ~ 3.27 Å. As the acceptor concentration increases, more serious π - π stacking and thus more severe energy loss can be anticipated. Therefore, all six exciplexes showed greater k_{nr} at when the acceptor concentration increases. Particularly, SAF-2NP-based exciplex emitters are less sensitive owing to the nearly perpendicular structure of SAF.

Table 2. Summary of EL performance based on the six exciplexes.

Device	Emitter	Weight Ratio	$V_{on}^{a)}$ [V]	$\lambda_{EL}^{b)}$ [nm]	Maximum CE/PE/EQE [cd A ⁻¹ /lm W ⁻¹ /%]	EQE ₁₀₀ /EQE ₅₀₀ /EQE ₁₀₀₀ ^{d)} [%]	CIE ^{b)} [x,y]
A1	mPTBC:SAF-2NP	9:1	3.3	608	41.5/34.7/23.8	19.3/14.5/12.1	(0.58, 0.42)
A2		8:2	3.1	616	31.2/27.2/21.9	17.6/13.4/11.2	(0.61, 0.39)
A3		7:3	3.0	620	26.8/24.0/21.1	17.1/13.3/11.3	(0.62, 0.38)
A4		6:4	3.0	624	24.3/21.8/20.7	17.3/13.4/11.3	(0.63, 0.37)
B	mPTZC:SAF-2NP	9:1	3.2	620	19.6/16.4/14.1	11.1/8.7/7.4	(0.60, 0.40)
C	mPTBC:TPA-2NP	9:1	2.9	596	24.3/25.8/12.5	5.3/3.9/3.4	(0.56, 0.43)
D	mPTBC:TPA-QP	9:1	3.1	612	13.3/13.5/9.34	3.7/2.5/2.1	(0.58, 0.41)
E	mPTZC:TPA-2NP	9:1	2.8	600	14.5/15.7/8.55	2.6/1.8/1.6	(0.56, 0.44)
F	mPTZC:TPA-QP	9:1	3.1	612	7.51/7.48/5.58	2.1/1.3/1.1	(0.56, 0.43)

^{a)} Driving voltage at 1 cd m⁻². ^{b)} At 500 cd m⁻². ^{c)} Maximum luminance. ^{d)} EQE at 100, 500 and 1000 cd m⁻².



OLED devices

Considering the dramatic contrast of the PL properties of the six exciplexes, their EL properties were then investigated. As shown in Figure 5A, a simple multi-layer device structure of ITO (110 nm)/TPAC (35 nm)/TCTA (10 nm)/emitting layer (EML, 20 nm)/TmPyPB (65 nm)/LiF (1 nm)/Al (100 nm) were used, where 4,4'-(cyclohexane-1,1-diyl)bis(N,N-di-p-tolyl-aniline) (TAPC), Tris(4-(9H-carbazol-9-yl)phenyl)amine (TCTA) and 3,3'-(5'-(3-(pyridin-3-yl)phenyl)-[1,1':3',1''-terphenyl]-3,3''-diyl)dipyridine (TmPyPB) were hole transporting, electron blocking and electron transporting layer, respectively (chemical structures see Figure S18). Indium tin oxide (ITO) and Al respectively serve as anode and cathode. LiF improved electron injection. Device A-F represent EML using mPTBC:SAF-2NP, mPTZC:SAF-2NP, mPTBC:TPA-2NP, mPTBC:TPA-QP, mPTZC:TPA-2NP and mPTZC:TPA-QP, respectively. As mentioned above, the D:A weight ratio was set to be 9:1 in the first place to suppress the π - π stacking of the acceptors. mPTBC:SAF-2NP-based OLEDs demonstrate the highest maximum luminance (Figure 5B), which can be ascribed to its superior structural stability. The higher electron transport ability of TPA-2NP endows TPA-2NP-based devices with higher current density than those based on TPA-QP (Figure S 19). According to the EL spectra in Figure 5C, all six exciplex-based OLEDs exhibited red emission peaked around 600 nm, similar to their PL spectra. Due to the serious non-radiative decay mainly induced by the flexible TPA group, devices D, E and F showed poor EQE_{max}s of 9.34%, 8.55% and 5.58%, respectively. Excitingly, device B and C demonstrated obvious performance enhancement and achieved maximum CE/PE/EQE of 24.3 cd A⁻¹/25.8 lm W⁻¹/12.5% and 19.6 cd A⁻¹/16.4 lm W⁻¹/14.1%, respectively (Figure 5D and Table 2). Consistent with what have been concluded from the PL properties, it is further verified that structural robustness is the priority in constructing high-performance red exciplex emitters, which is demonstrated by more significant improvements after rigidifying the molecules (from mPTZC:TPA-2NP to mPTZC:SAF-2NP), as compared with introducing HBs (from mPTBC:TPA-QP to mPTBC:TPA-2NP). The proof-of-concept mPTBC:SAF-2NP achieved exceptional maximum CE, PE and EQE of 41.5 cd A⁻¹, 34.7 lm W⁻¹ and 23.8%, respectively, showing a 4.2-fold improvement in EQE_{max} compared with mPTZC:TPA-QP. These results not only take a huge lead to previously reported red OLEDs based on exciplex emitters (Figure 5E)⁴¹⁻⁴⁶ but also ranks among the state-of-the-art exciplex-emissive OLEDs (Figure S20, Table S6). Further, OLEDs with different D:A mixing ratios were then fabricated to study the effect of D-D/A-A interactions on device performances. For mPTBC:SAF-2NP, device A1-A4 were fabricated with D:A ratios of 9:1, 8:2, 7:3 and 6:4, respectively. The spectra redshifts are the synergistic effect of increased π - π interactions of SAF-2NP, and the self-polarization-induced solid-state solvation effect caused by larger dipole moments of SAF-2NP (1.80 Debye) than mPTBC (0.055 Debye).²⁹ The EQE_{max}s gradually decrease as the increasing of acceptor concentration (Figure S21, Table 2), showing a similar trend as in photophysical studies, which should be ascribed to exciton quenching due to the π - π interactions of SAF-2NP. Despite this, EQE_{max}s of the

four devices remain above 20% with emission peaks ranging from 608 to 624 nm, demonstrating superiority to those concentration-sensitive single-component TADF red emitters.^{29,30,47-49} The device performances based on other five emitters with different D:A mixing ratio are shown in Figure S22, S23 and Table S5. Similarly, mPTZC:SAF-2NP also shows moderate concentration quenching with EQE_{max}s decrease from 14.1% to 11.9% as the acceptor concentration increases to 20%. Conversely, TPA-containing exciplex emitters demonstrate significant EQE_{max} decline with drop rates ranging from 45.7% to 56.7%, indicating that TPA-based acceptors are much more sensitive to concentration and are prone to π - π stacking, which is consistent with their photophysical properties. Based on the above studies, the outstanding performance of device A1 is the result of effectively suppressing the non-radiative decay, including 1) applying stiff structures of the spiro-locked acceptor and the sterically restricted donor that minimize structural relaxation, 2) introducing intermolecular HBs that optimize the D-A interactions and 3) fine-tuned D:A weight ratios which constrains concentration quenching. Apart from the higher EQE_{max}s, it is noteworthy that device A1 and B had small efficiency roll-offs of 18.9%/39.1%/49.2% and 21.3%/38.3%/47.5%, respectively, at 100/500/1000 cd m⁻². In sharp contrast, EQEs of device C-F decreased much faster that drop rates of EQE₁₀₀ vary from 57.6% to 69.6%, which can be ascribed to the triplet-triplet annihilation and triplet-polaron annihilation induced by longer τ_d of TPA-2NP- and TPA-QP-based exciplexes.

To demonstrate the positive effect of TADF-characterized components on the exciton utilization, 11-([1,1':3',1''-terphenyl]-5'-yl)dipyrido[3,2-a:2',3'-c]phenazine (TPh-2NP) was designed and synthesized for comparison purposes (Figure S24) by replacing TPA with terphenyl. Only nanosecond-scale lifetime was observed, suggesting its locally-excited characteristic. Demonstrating similar rigidity compared with TPA-2NP (Figure S24a; the relatively small RMSD_{S₁-T₁} may be due to both S₁ and T₁ being locally excited states), the EQE_{max} of mPTBC:TPh-2NP based device is 5.2 %, less than half of that of mPTBC:TPA-2NP (Figure S25), indicating that the introduction of TADF components greatly improves the exciton utilization.⁵⁰ Compared with blue and green emission, such positive effect may be amplified in the long-wavelength region where the non-radiative decay becomes overwhelming.^{8,16}

Finally, the operational stability of the six exciplex emitters was studied using a device structure of ITO/NPB (40 nm)/Tris-PCz (10 nm)/EML (20 nm)/SF3-TRZ(10 nm)/SF3-TRZ:Liq (7:3, 50 nm)/Liq (2 nm)/Al (100 nm). The EML is consistent with device A1 and B-F. As shown in Figure S26, LT₅₀ (time corresponds to 50% of the initial luminance) at 500 cd m⁻² of mPTBC:SAF-2NP, mPTZC:SAF-2NP, mPTBC:TPA-2NP, mPTBC:TPA-QP, mPTZC:TPA-2NP and mPTZC:TPA-QP are 349, 213, 186, 157, 153 and 92 hours, following the same trend as their EQE_{max}s in Table 2. The longer lifetimes of SAF-2NP-based exciplex emitters may originate from their shorter exciton lifetimes⁵¹ as mentioned in the photophysical study.



Conclusions

In conclusion, we have elucidated that the rigidity of molecular structures, the interactions between D and A molecules as well as D-D/A-A interactions are influential to the non-radiative decay of exciplex emitters. By constructing a rigid system featuring stiff structures that inhibit structural relaxation, HBs which optimize intermolecular interactions and a fine-tuned D:A mixing ratio, the proof-of-concept exciplex emitter mPTBC:SAF-2NP showed a 3.3-fold higher Φ_{PL} (84.1%) and a 70% lower k_{nr} ($1.98 \times 10^6 \text{ s}^{-1}$) than the comparison group. mPTBC:SAF-2NP also achieved outstanding EL performance, showing a superior EQE_{max} of 23.8% with an emission peak of 608 nm, which represents a significant advancement over previously reported red OLEDs based on exciplex emitters. The present work provides a comprehensive understanding of non-radiative decay paths of exciplex emitters and can be a guide for developing efficient multicomponent emitting systems.

Author Contributions

H.-Y.Z. led the investigation, formal analysis and wrote the original draft. M.Z. and H.Z. helped with the data curation and validation. H.-Y.Y. helped with the investigation (synthesis). B.H. contributed to formal analysis and funding acquisition. Y.-H.Z. contributed to formal analysis and methodology. H.W. helped with the methodology. S.-L.T. and H.L. helped review and edit the manuscript. C.-J.Z. conceptualized, supervised and funded the project. X.-H.Z. helped review the manuscript and provided fund.

Conflicts of interest

There are no conflicts to declare.

Data availability

All experimental and calculational data are available from the corresponding author upon reasonable request.

Acknowledgements

This work was supported by the National Natural Science Foundation of China (Grant Nos. 62222503, 52073040 and 52130304), the Sichuan Science and Technology Program (Grant Nos. 2024NSFSC0012 and 2023NSFSC1973), the Collaborative Innovation Center of Suzhou Nano Science & Technology, and the Open Research Fund of Chengdu University of Traditional Chinese Medicine State Key Laboratory Southwestern Chinese Medicine Resources (SKLTCM202303).

Notes and references

- 1 B. Hu, Z. Yang and F. E. Karasz, *J. Appl. Phys.*, 1994, **76**, 2419–2422.
- 2 K. Goushi, K. Yoshida, K. Sato and C. Adachi, *Nat. Photonics*, 2012, **6**, 253–258.
- 3 M. Zhang, C.-J. Zheng, H. Lin and S.-L. Tao, *Mater. Horiz.*, 2021, **8**, 401–425.

- 4 M. Sarma, L.-M. Chen, Y.-S. Chen and K.-T. Wong, *Mater. Sci. Eng. R Rep.*, 2022, **150**, 100689. DOI: 10.1039/D4SC03667K
- 5 X.-K. Liu, Z. Chen, C.-J. Zheng, C.-L. Liu, C.-S. Lee, F. Li, X.-M. Ou and X.-H. Zhang, *Adv. Mater.*, 2015, **27**, 2378–2383.
- 6 M. Wang, Y. Huang, K. Lin, T. Yeh, J. Duan, T. Ko, S. Liu, K. Wong and B. Hu, *Adv. Mater.*, 2019, **31**, 1904114.
- 7 T.-C. Lin, M. Sarma, Y.-T. Chen, S.-H. Liu, K.-T. Lin, P.-Y. Chiang, W.-T. Chuang, Y.-C. Liu, H.-F. Hsu, W.-Y. Hung, W.-C. Tang, K.-T. Wong and P.-T. Chou, *Nat. Commun.*, 2018, **9**, 3111.
- 8 M. Zhang, W. Liu, C. Zheng, K. Wang, Y. Shi, X. Li, H. Lin, S. Tao and X. Zhang, *Adv. Sci.*, 2019, **6**, 1801938.
- 9 J. Zhao, C. Zheng, Y. Zhou, C. Li, J. Ye, X. Du, W. Li, Z. He, M. Zhang, H. Lin, S. Tao and X. Zhang, *Mater. Horiz.*, 2019, **6**, 1425–1432.
- 10 Z. Zhang, D. Dou, R. Xia, P. Wu, E. Spuling, K. Wang, J. Cao, B. Wei, X. Li, J. Zhang, S. Bräse and Z. Wang, *Sci. Adv.*, 2023, **9**, eadf4060.
- 11 N. R. Al Amin, K. K. Kesavan, S. Biring, C.-C. Lee, T.-H. Yeh, T.-Y. Ko, S.-W. Liu and K.-T. Wong, *ACS Appl. Electron. Mater.*, 2020, **2**, 1011–1019.
- 12 T.-L. Wu, S.-Y. Liao, P.-Y. Huang, Z.-S. Hong, M.-P. Huang, C.-C. Lin, M.-J. Cheng and C.-H. Cheng, *ACS Appl. Mater. Interfaces*, 2019, **11**, 19294–19300.
- 13 Y. Qin, P. Tao, L. Gao, P. She, S. Liu, X. Li, F. Li, H. Wang, Q. Zhao, Y. Miao and W. Huang, *Adv. Opt. Mater.*, 2019, **7**, 1801160.
- 14 W.-Y. Hung, G.-C. Fang, S.-W. Lin, S.-H. Cheng, K.-T. Wong, T.-Y. Kuo and P.-T. Chou, *Sci. Rep.*, 2014, **4**, 5161.
- 15 M. Zhang, C.-J. Zheng, H.-Y. Zhang, H.-Y. Yang, K. Wang, Y.-Z. Shi, H. Lin, S.-L. Tao and X.-H. Zhang, *J. Mater. Chem. C*, 2022, **10**, 15593–15600.
- 16 Y. Hu, Y. Yu, Y. Yuan, Z. Jiang and L. Liao, *Adv. Opt. Mater.*, 2020, **8**, 1901917.
- 17 R. Englman and J. Jortner, *Mol. Phys.*, 1970, **18**, 145–164.
- 18 J. H. Kim, J. H. Yun and J. Y. Lee, *Adv. Opt. Mater.*, 2018, **6**, 1800255.
- 19 Q. Zhang, H. Kuwabara, W. J. Potscavage, S. Huang, Y. Hatae, T. Shibata and C. Adachi, *J. Am. Chem. Soc.*, 2014, **136**, 18070–18081.
- 20 H.-Y. Yang, H. Zhang, M. Zhang, X. Fan, H. Lin, S.-L. Tao, C.-J. Zheng and X.-H. Zhang, *Chem. Eng. J.*, 2022, **448**, 137717.
- 21 C.-Y. Lin, C.-H. Hsu, C.-M. Hung, C.-C. Wu, Y.-H. Liu, E. H.-C. Shi, T.-H. Lin, Y.-C. Hu, W.-Y. Hung, K.-T. Wong and P.-T. Chou, *Nat. Chem.*, 2024, **16**, 98–106.
- 22 A. Chand, D. K. Sahoo, A. Rana, S. Jena and H. S. Biswal, *Acc. Chem. Res.*, 2020, **53**, 1580–1592.
- 23 S. Emamian, T. Lu, H. Kruse and H. Emamian, *J. Comput. Chem.*, 2019, **40**, 2868–2881.
- 24 R. Lin, J. Liu, W. Xu, Z. Liu, X. He, C. Zheng, M. Kang, X. Li, Z. Zhang, H.-T. Feng, J. W. Y. Lam, D. Wang, M. Chen and B. Z. Tang, *Adv. Mater.*, 2023, **35**, 2303212.
- 25 D.-Q. Wang, M. Zhang, K. Wang, C.-J. Zheng, Y.-Z. Shi, J.-X. Chen, H. Lin, S.-L. Tao and X.-H. Zhang, *Dyes Pigments*, 2017, **143**, 62–70.
- 26 H.-Y. Zhang, H.-Y. Yang, M. Zhang, H. Lin, S.-L. Tao, C.-J. Zheng and X.-H. Zhang, *Mater. Horiz.*, 2022, **9**, 2425–2432.
- 27 C. B. Larsen, H. van der Salm, C. A. Clark, A. B. S. Elliott, M. G. Fraser, R. Horvath, N. T. Lucas, X.-Z. Sun, M. W. George and K. C. Gordon, *Inorg. Chem.*, 2014, **53**, 1339–1354.
- 28 C. Si, A. K. Gupta, B. Basumatary, A. P. McKay, D. B. Cordes, A. M. Z. Slawin, I. D. W. Samuel and E. Zysman-Colman, *Adv. Funct. Mater.*, 2024, **34**, 2315935.
- 29 J. Xue, Q. Liang, R. Wang, J. Hou, W. Li, Q. Peng, Z. Shuai and J. Qiao, *Adv. Mater.*, 2019, **31**, 1808242.
- 30 C. Li, R. Duan, B. Liang, G. Han, S. Wang, K. Ye, Y. Liu, Y. Yi and Y. Wang, *Angew. Chem. Int. Ed.*, 2017, **56**, 11525–11529.
- 31 M. Cocchi, D. Virgili, G. Giro, V. Fattori, P. Di Marco, J. Kalinowski and Y. Shirota, *Appl. Phys. Lett.*, 2002, **80**, 2401–2403.



32 M. J. Frisch, G. W. Trucks, H. B. Schlegel, G. E. Scuseria, M. A. Robb, J. R. Cheeseman, G. Scalmani, V. Barone, G. A. Petersson, H. Nakatsuji, X. Li, M. Caricato, A. V. Marenich, J. Bloino, B. G. Janesko, R. Gomperts, B. Mennucci, H. P. Hratchian, J. V. Ortiz, A. F. Izmaylov, J. L. Sonnenberg, Williams, F. Ding, F. Lipparini, F. Egidi, J. Goings, B. Peng, A. Petrone, T. Henderson, D. Ranasinghe, V. G. Zakrzewski, J. Gao, N. Rega, G. Zheng, W. Liang, M. Hada, M. Ehara, K. Toyota, R. Fukuda, J. Hasegawa, M. Ishida, T. Nakajima, Y. Honda, O. Kitao, H. Nakai, T. Vreven, K. Throssell, J. A. Montgomery Jr., J. E. Peralta, F. Ogliaro, M. J. Bearpark, J. J. Heyd, E. N. Brothers, K. N. Kudin, V. N. Staroverov, T. A. Keith, R. Kobayashi, J. Normand, K. Raghavachari, A. P. Rendell, J. C. Burant, S. S. Iyengar, J. Tomasi, M. Cossi, J. M. Millam, M. Klene, C. Adamo, R. Cammi, J. W. Ochterski, R. L. Martin, K. Morokuma, O. Farkas, J. B. Foresman and D. J. Fox, *Gaussian 16 Rev. A.03.*, Wallingford, CT, 2016.

34 J. R. Reimers, *J. Chem. Phys.*, 2001, **115**, 9103–9109.

35 M. Zhang, C. Zheng, K. Wang, Y. Shi, D. Wang, X. Li, H. Lin, S. Tao and X. Zhang, *Adv. Funct. Mater.*, 2021, **31**, 2010100.

36 X. Du, X. Lu, J. Zhao, Y. Zhang, X. Li, H. Lin, C. Zheng and S. Tao, *Adv. Funct. Mater.*, 2019, **29**, 1902078.

37 T. Lu and Q. Chen, *J. Comput. Chem.*, 2022, **43**, 539–555.

38 T. Lu and F. Chen, *J. Comput. Chem.*, 2012, **33**, 580–592.

39 J. Zhang and T. Lu, *Phys. Chem. Chem. Phys.*, 2021, **23**, 20323–20328.

40 V. Jankus, P. Data, D. Graves, C. McGuinness, J. Santos, M. R. Bryce, F. B. Dias and A. P. Monkman, *Adv. Funct. Mater.*, 2014, **24**, 6178–6186.

41 W.-Y. Hung, G.-C. Fang, Y.-C. Chang, T.-Y. Kuo, P.-T. Chou, S.-W. Lin and K.-T. Wong, *ACS Appl. Mater. Interfaces*, 2013, **5**, 6826–6831.

42 B. Zhao, T. Zhang, B. Chu, W. Li, Z. Su, Y. Luo, R. Li, X. Yan, F. Jin, Y. Gao and H. Wu, *Org. Electron.*, 2015, **17**, 15–21.

43 D. Chen, G. Xie, X. Cai, M. Liu, Y. Cao and S. Su, *Adv. Mater.*, 2016, **28**, 239–244.

44 G. Grybauskaite-Kaminskiene, K. Ivaniuk, G. Bagdziunas, P. Turyk, P. Stakhira, G. Baryshnikov, D. Volyniuk, V. Cherpak, B. Minaev, Z. Hotra, H. Ågren and J. V. Grazulevicius, *J. Mater. Chem. C*, 2018, **6**, 1543–1550.

45 G. Liu, T. Huang, H. Wang, C. Hsu, P. Chou, W. Hung and K. Wong, *Chem. – Eur. J.*, 2023, **29**, e202203660.

46 M. Chapran, P. Pander, M. Vasylieva, G. Wiosna-Salyga, J. Ulanski, F. B. Dias and P. Data, *ACS Appl. Mater. Interfaces*, 2019, **11**, 13460–13471.

47 Y. Zhang, Q. Ran, Q. Wang, Y. Liu, C. Hänisch, S. Reineke, J. Fan and L. Liao, *Adv. Mater.*, 2019, **31**, 1902368.

48 Z. Cai, X. Wu, H. Liu, J. Guo, D. Yang, D. Ma, Z. Zhao and B. Z. Tang, *Angew. Chem. Int. Ed.*, 2021, **60**, 23635–23640.

49 H. Wang, K. Wang, J. Chen, X. Zhang, L. Zhou, X. Fan, Y. Cheng, X. Hao, J. Yu and X. Zhang, *Adv. Funct. Mater.*, 2023, **33**, 2304398.

50 W. Liu, J.-X. Chen, C.-J. Zheng, K. Wang, D.-Y. Chen, F. Li, Y.-P. Dong, C.-S. Lee, X.-M. Ou and X.-H. Zhang, *Adv. Funct. Mater.*, 2016, **26**, 2002–2008.

51 L.-S. Cui, A. J. Gillett, S.-F. Zhang, H. Ye, Y. Liu, X.-K. Chen, Z.-S. Lin, E. W. Evans, W. K. Myers, T. K. Ronson, H. Nakanotani, S. Reineke, J.-L. Bredas, C. Adachi and R. H. Friend, *Nat. Photonics*, 2020, **14**, 636–642.

View Article Online
DOI: 10.1039/D4SC03667K



Data availability statements

View Article Online
DOI: 10.1039/D4SC03667K

All experimental and calculational data are available from the corresponding author upon reasonable request.

